CHEMISTRY
A EUROPEAN JOURNAL

Expanding the World of Endohedral Fullerenes—The $Tm_3N@C_{2n}$ ($39 \leq n \leq 43$) Clusterfullerene Family

Matthias Krause,* Joanna Wong, and Lothar Dunsch[a]

Abstract: A new family of endohedral fullerenes, based on an encaged trithulium nitride (Tm_3N) cluster, was synthesised, isolated and characterised by HPLC, mass spectrometry, and visible-NIR and FTIR spectroscopy. Tm_3N clusterfullerenes with cages as small as C_{76} and as large as C_{88} were prepared and six of them were isolated. $Tm_3N@C_{78}$ is a small clusterfullerene. The two isomers of $Tm_3N@C_{80}$ (I and II) were the most abundant structures in the fullerene soot. $Tm_3N@C_{82}$, $Tm_3N@C_{84}$, and $Tm_3N@C_{86}$ represent a new series of higher clusterfullerenes. All six isolated Tm_3N clusterfullerenes were classified as large energy-gap structures with optical energy gaps between ~1.2 and ~1.75 eV. $Tm_3N@C_{80}$ (I) and $Tm_3N@C_{80}$ (II) were assigned to the C_{80} cages C_{80}:7 (I_h) and C_{80}:6 (D_{5h}). For $Tm_3N@C_{78}$, the analysis pointed to an elliptical carbon cage with C_{78}:1 (D_3) or C_{78}:4 (D_{3h}) being the probable structures.

Keywords: fullerenes · high-pressure liquid chromatography · IR spectroscopy · mass spectrometry · thulium

Introduction

Endohedral fullerenes are a relatively new class of compounds. They are composed of encaged atoms, ions, or clusters within a closed carbon cage. Both the host fullerenes and the encaged species show a variety of unexpected electronic and structural properties.[1,2] In fact, many fullerene cages are accessible only in endohedral form, as for example, the IPR-obeying C_{74} (IPR = isolated pentagon rule) and the non-IPR fullerene C_{66}.[3,4] In endohedral monometallofullerenes the encaged rare earth element thulium has a valence state of +2, whereas it exhibits a +3 valence state in the metal and usually also in solution and in coordination compounds.[5,6] Another remarkable property of endohedral fullerenes is their ability to stabilise reactive species as in the cases of atomic nitrogen in $N@C_{60}$ or a trigonal Sc_3 cluster in $Sc_3@C_{82}$.[7–10]

The discovery of $Sc_3N@C_{80}$ in 1999 opened the gate to a new class of endohedral fullerenes with an encaged trimetal nitride cluster.[11] Trimetal nitride clusterfullerenes are distinguished by several promising properties, for example, outstanding high yields relative to empty, mono- and dimetallofullerenes, a high thermal stability and a long term stability in air.[11–15] Currently scandium is the most commonly used metal in the synthesis of trimetal nitride clusterfullerenes. The Sc_3N family consists of $Sc_3N@C_{80}$, $Sc_3N@C_{78}$, and $Sc_3N@C_{68}$.[11,16,17] All other known trimetal nitride clusterfullerenes including Y_3N,[15] Tb_3N,[18] Lu_3N[19] and Ho_3N,[13] and the mixed metal clusters $ErSc_2N$[20] and Er_2ScN[14] have been limited to a C_{80} fullerene cage.

Recently a second isomer of $Sc_3N@C_{80}$ based on a D_{5h} C_{80} cage was discovered.[21] Both $Sc_3N@C_{80}$ isomers (I and II) were separated and characterised by optical and vibrational spectroscopy.[22] It is important to clarify whether a similar coexistence of two cage isomers exists in other $M_3N@C_{80}$ clusterfullerene samples. Another open question worth addressing is whether clusterfullerenes with cages different to those presently known can be prepared and isolated.

In this paper the isolation of six new clusterfullerenes, the $Tm_3N@C_{2n}$ ($39 \leq n \leq 43$) family, is reported. Their chemical identity and purity were established by mass spectrometry. The optical energy gaps and the electronic absorptions were determined by visible-NIR spectroscopy. The cage isomers of $Tm_3N@C_{80}$ (I), $Tm_3N@C_{80}$ (II), and $Tm_3N@C_{78}$ were analysed by chromatographic retention times, and visible-NIR and FTIR spectroscopy.

[a] Dr. M. Krause, J. Wong, Prof. Dr. L. Dunsch
Leibniz-Institute for Solid State and Materials Research Dresden
Institute of Solid State Research
Group of Electrochemistry and Conducting Polymers
Postfach 270116, 01171 Dresden (Germany)
Fax: (+49) 351-465-9745
E-mail: m.krause@ifw-dresden.de

DOI: 10.1002/chem.200400673

Results and Discussion

The chromatogram and the mass spectrum of the fullerene extract give evidence for the formation of Tm_3N clusterfullerenes with cages as small as C_{76} and as large as C_{88} (Figure 1). $Tm_3N@C_{80}$ represents the most abundant fraction in the fullerene extract. Among the Tm3N clusterfullerenes

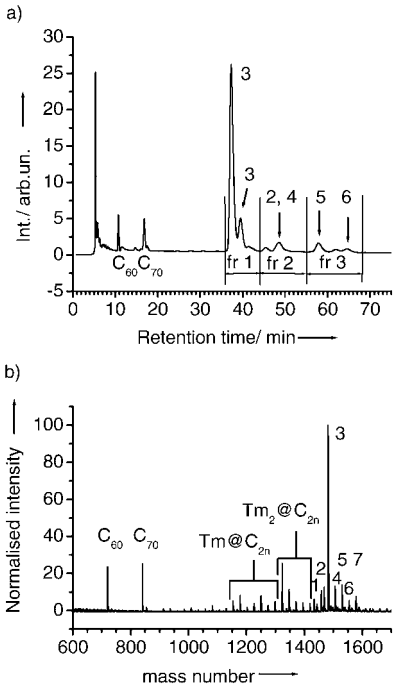

Figure 1. a) Chromatogram of the Tm_3N fullerene extract and scheme of the first separation stage into three main fractions labelled fr 1, fr 2 and fr 3. The sharp peak around 5 min is due to hydrocarbon byproducts. b) Positive ion LD-TOF mass spectrum of the fullerene extract. The numbers in both a) and b) label the following Tm_3N fullerenes: 1 = $Tm_3N@C_{76}$, 2 = $Tm_3N@C_{78}$, 3 = $Tm_3N@C_{80}$, 4 = $Tm_3N@C_{82}$, 5 = $Tm_3N@C_{84}$, 6 = $Tm_3N@C_{86}$, 7 = $Tm_3N@C_{88}$.

$Tm_3N@C_{84}$ was the second most abundant. Furthermore, $Tm_3N@C_{78}$, $Tm_3N@C_{82}$ and $Tm_3N@C_{86}$ were formed with smaller but still separable amounts. $Tm_3N@C_{76}$ and $Tm_3N@C_{88}$ were detected in the extract. In addition to trithulium nitride and empty fullerenes, thulium mono- and dimetallofullerenes, $Tm@C_{2n}$ ($41 \leq n \leq 47$) and $Tm_2@C_{2n}$ ($41 \leq n \leq 46$), were detected.

Chemical identities and purities of the isolated Tm_3N clusterfullerenes were established by the chromatograms and mass spectra given in Figures 2 and 3. The isolated Tm_3N clusterfullerenes, like other endohedral structures, were stable throughout the chromatographic separation and under laser desorption time-of-flight (LD-TOF) conditions. The sample purities were ~99% for $Tm_3N@C_{78}$, ≥99% for $Tm_3N@C_{80}$ (I and II), ≥90% for $Tm_3N@C_{82}$, ≥95% for $Tm_3N@C_{84}$ and ~80% for $Tm_3N@C_{86}$. The last sample contained some nonseparable $Tm_3N@C_{88}$ as the main impurity. The presence of oxides could be ruled out. As in the case of the Sc_3N clusterfullerenes,[21,22] two stable C_{80} based structures exist for Tm_3N. The minor $Tm_3N@C_{80}$ (II) isomer made up 15–20% of the entire $Tm_3N@C_{80}$ fraction. This is the same content as that of $Sc_3N@C_{80}$ (II) in the whole $Sc_3N@C_{80}$ fraction.[22]

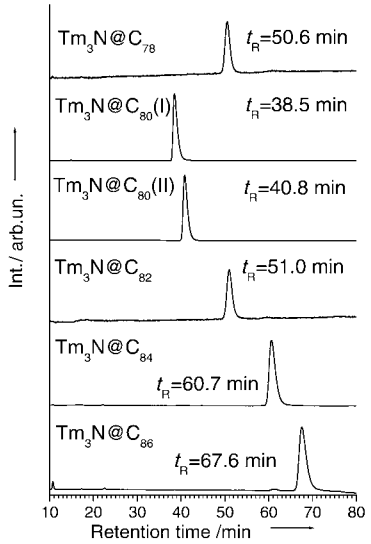

Figure 2. Chromatograms of isolated $Tm_3N@C_{78}$, $Tm_3N@C_{80}$ (I and II), $Tm_3N@C_{82}$, $Tm_3N@C_{84}$ and $Tm_3N@C_{86}$; linear combination of two 4.6 × 250 mm Buckyprep columns; flow rate 1.6 mL min^{-1}, injection volume 100 μL, 30 °C.

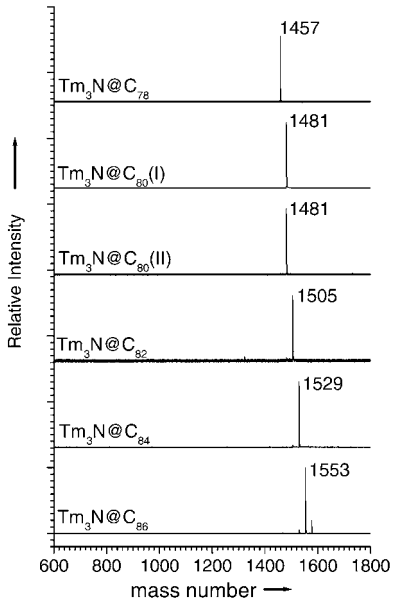

Figure 3. Positive ion LD-TOF mass spectra of isolated $Tm_3N@C_{78}$, $Tm_3N@C_{80}$ (I and II), $Tm_3N@C_{82}$, $Tm_3N@C_{84}$ and $Tm_3N@C_{86}$.

Under identical experimental conditions, the retention times of the major and the minor $Tm_3N@C_{80}$ isomer are very similar to those of the $Sc_3N@C_{80}$ isomers I and II: 38.5 min and 40.8 min for the Tm_3N clusterfullerenes compared to 38.8 and 40.5 min for the Sc_3N clusterfullerenes.[22] This is a strong indication that the electronic and geometric

structures are similar to those of $Sc_3N@C_{80}$ (I and II). This correlation implies a charge transfer of six electrons from the Tm_3N cluster to the C_{80} cages and an almost spherical charge distribution of the fullerene. However, even after accounting for a charge transfer of six electrons, the retention times of the other four Tm_3N clusterfullerenes are much too high, indicating significant contributions of dipole–dipole and quadrupole–quadrupole interactions to the overall retention time. This is particularly pronounced for $Tm_3N@C_{78}$. Its retention time of 50.6 min is much greater than that of $Sc_3N@C_{78}$ (36.6 min)[22] and would suggest an incredible charge transfer of 13 electrons. Aberrantly high dipole and/or quadrupole moments are presumably responsible for the very large retention time of $Tm_3N@C_{78}$. A nonspherical charge distribution caused by an elongated elliptical cage, the likeliest examples being C_{78}:1 (D_3) or C_{78}:4 (D_{3h}),[23] can account for the retention behaviour of $Tm_3N@C_{78}$.

Visible-NIR spectra of $Tm_3N@C_{80}$ (I), $Tm_3N@C_{80}$ (II), and $Tm_3N@C_{78}$ are presented along with those of their Sc_3N counterparts in Figure 4, and those of the three higher Tm_3N clusterfullerenes are shown in Figure 5 below. Selected visible-NIR data are listed in Table 1. No absorptions beyond 1100 nm were observed for the Tm_3N clusterfullerene family members. The lowest energetic transitions, which are the measure for the optical energy gap, were found between 1.18 eV for $Tm_3N@C_{86}$ and 1.76 eV for $Tm_3N@C_{80}$ (I). Since an energy gap value of 1.0 eV marks the borderline between large and low energy-gap fullerenes, the isolated $Tm_3N@C_{2n}$ family members are classified as large energy-gap fullerenes. To some extent the energy-gap ordering of the Tm_3N clusterfullerenes can be correlated with their abundance in the fullerene soot. Both $Tm_3N@C_{80}$ isomers have significantly larger energy gaps and are formed in greater abundance than $Tm_3N@C_{84}$, which in turn has a larger gap and higher abundance than $Tm_3N@C_{86}$. Only $Tm_3N@C_{78}$ and $Tm_3N@C_{82}$ are less abundant than expected from their energy gaps, which are of the same order as that of $Tm_3N@C_{80}$ (II). These exceptions could be due to kinetic reasons, as no thermodynamic equilibrium is established during the fullerene formation. Hence it seems possible, that the most abundant $Tm_3N@C_{80}$ (I) clusterfullerene is formed at the cost of the nearest neighbour cage sizes $Tm_3N@C_{78}$ and $Tm_3N@C_{82}$.

For structure analysis of the isolated $Tm_3N@C_{2n}$ clusterfullerenes, the isolated pentagon isomers have to be considered in a first approximation, that is, 5 C_{78}, 7 C_{80}, 9 C_{82}, 24 C_{84}, and 19 C_{86} cages. In order to reveal similarities and differences in the carbon cage structures, the visible-NIR signatures of $Tm_3N@C_{80}$ (I), $Tm_3N@C_{80}$ (II) and $Tm_3N@C_{78}$ were compared to those of their Sc_3N counterparts (Figure 4). These

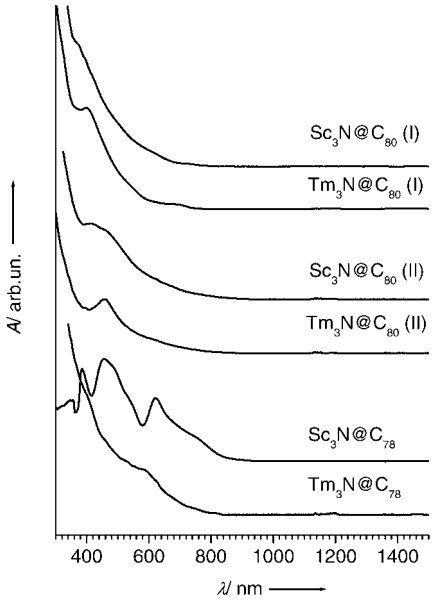

Figure 4. Visible-NIR spectra of $Tm_3N@C_{80}$ (I), $Tm_3N@C_{80}$ (II) and $Tm_3N@C_{78}$ dissolved in toluene, 10 mm path length, 2 nm resolution in comparison to the response of $Sc_3N@C_{80}$ (I), $Sc_3N@C_{80}$ (II), and $Sc_3N@C_{78}$.

Table 1. Characteristic visible-NIR absorptions and absorption onset of $Tm_3N@C_{78}$, $Tm_3N@C_{80}$ (I) and (II), $Tm_3N@C_{82}$, $Tm_3N@C_{84}$ and $Tm_3N@C_{86}$.

	$Tm_3N@C_{78}$ λ [nm]	$Tm_3N@C_{80}$ (I) λ [nm]	$Tm_3N@C_{80}$ (II) λ [nm]	$Tm_3N@C_{82}$ λ [nm]	$Tm_3N@C_{84}$ λ [nm]	Tm3 N@C_{86} λ [nm]
strongest absorptions	400 sh	407 m	460 s	490 sh	480 sh	460 m
	590 sh	540 sh	625 sh	620 sh	610 m	590 m
		675 w	710 sh			710 sh
lowest energetic absorption	750 w	705 w	820 vw	750 vw	900 vw	1050 vw
onset	850	780	900	950	1050	1250

absorptions are predominantly due to π–π^* carbon-cage transitions and depend on the carbon-cage geometry and its charge state. For $Tm_3N@C_{80}$ (I) and $Sc_3N@C_{80}$ (I) only slightly different wavelengths were observed for the absorption onset, the lowest energetic absorption and the strongest visible-NIR absorptions: 780 and 820 nm, 705 and 735 nm, and 407 and a band pair centred at 401 nm, respectively. A close resemblance was also found between the visible-NIR spectra of $Tm_3N@C_{80}$ (II) and $Sc_3N@C_{80}$ (II): the onsets were 900 and 920 nm, the longest wavelength absorptions appeared at 820 and 780 nm, respectively; the strongest absorption of $Tm_3N@C_{80}$ (II) at 460 nm can be correlated with the medium intense $Sc_3N@C_{80}$ (II) absorptions at 472 and 426 nm. Significant differences were found between the visible-NIR spectra of $Tm_3N@C_{78}$ and $Sc_3N@C_{78}$. The first was observed in the spectral range around 400 nm, at which the Tm_3N compound showed a medium intense absorption band, whereas $Sc_3N@C_{78}$ exhibited an absorption minimum.

A second discrepancy was found around 600 nm, at which the $Tm_3N@C_{78}$ spectrum showed a medium intense absorption band at 590 nm, whereas an absorption minimum was found for $Sc_3N@C_{78}$. From these comparisons, the visible-NIR signatures indicate that $Tm_3N@C_{80}$ (I) and $Sc_3N@C_{80}$ (I) as well as $Tm_3N@C_{80}$ (II) and $Sc_3N@C_{80}$ (II) have similar carbon cages and electronic structures. On the other hand these comparisons imply different cage structures for $Tm_3N@C_{78}$ and $Sc_3N@C_{78}$, as indicated first by their extremely different HPLC retention times.

No trimetal nitride clusterfullerenes higher than C_{80} have been isolated and characterised so far. Hence, the visible-NIR signatures of $Tm_3N@C_{82}$, $Tm_3N@C_{84}$ and $Tm_3N@C_{86}$ (Figure 5) were compared to those of endohedral dimetallo-

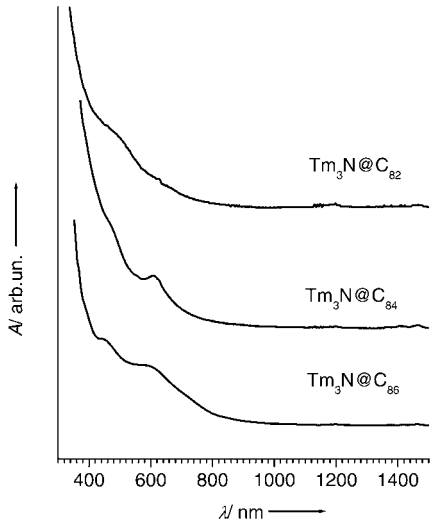

Figure 5. Visible-NIR spectra of $Tm_3N@C_{82}$, $Tm_3N@C_{84}$ and $Tm_3N@C_{86}$, parameters as in Figure 4.

fullerenes: $Tm_2@C_{82}$ (I, II, III),[24] $Er_2@C_{82}$ (I, III),[24] $Sc_2@C_{84}$ (I: C_s, II: C_{2v}, III: D_{2d}),[25] $Dy_2@C_{84}$ (I, III),[26] $Sc_2@C_{86}$ (II)[27] and $Er_2@C_{86}$ (I, II, III).[28] No reasonable correspondence was found between the Tm_3N clusterfullerene spectra and those of the dimetallofullerenes. How this conclusion was achieved is illustrated in detail for the C_{84}-based fullerenes. $Sc_2@C_{84}$ (I, II) and $Dy_2@C_{84}$ (I) have NIR absorptions at 1200 nm and 1750 nm, respectively, and their onsets are at around 1400 and 2000 nm.[25,26] $Sc_2@C_{84}$ (III) and $Dy_2@C_{84}$ (III) exhibit a strong NIR absorption at 880 nm and an onset at around 1200 nm. These signatures are characteristic for the C_{84} dimetallofullerenes. $Tm_3N@C_{84}$ has no NIR absorptions and an onset of 1050 nm. It might be indicated that different carbon cages can be stabilised depending on whether two metal ions or a trimetal nitride cluster are present in the formation process.

FTIR spectroscopy in combination with group theory provides direct structural information about the carbon cage and the encaged trimetal nitride cluster.[15,22] The FTIR spectra of $Tm_3N@C_{80}$ (I), $Tm_3N@C_{80}$ (II) and $Tm_3N@C_{78}$ are displayed in Figure 6 along with the spectra of $Sc_3N@C_{80}$ (I),[22]

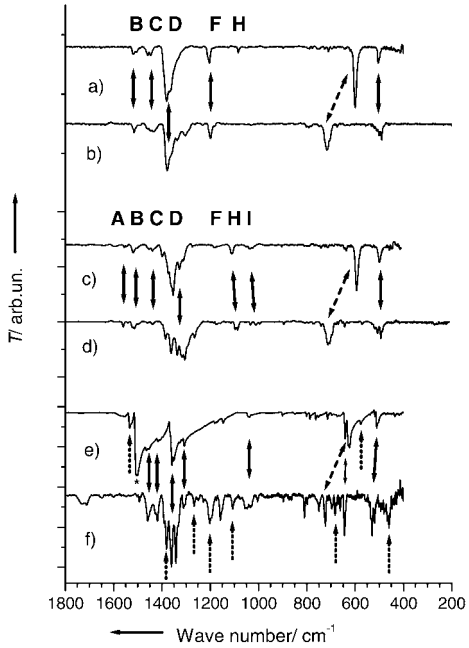

Figure 6. FTIR spectra of a) $Sc_3N@C_{80}$ (I), b) $Tm_3N@C_{80}$ (I), c) $Sc_3N@C_{80}$ (II), d) $Tm_3N@C_{80}$ (II), e) $Sc_3N@C_{78}$ and f) $Tm_3N@C_{78}$; 500 accumulations, 2 cm^{-1} resolution; capital letters refer to the line group classification introduced for $Sc_3N@C_{80}$ in references [15,22]; the corresponding line groups of $M_3N@C_{80}$ (M = Sc, Tm) isomers (I) and $M_3N@C_{80}$ (M = Sc, Tm) isomers (II) are marked by solid arrows; the dashed arrows indicate the ν_{as}(ScN, TmN) mode shift; fingerprint lines of $Tm_3N@C_{78}$ and $Sc_3N@C_{78}$ are marked by dotted arrows; a CS_2 mode in the spectrum of $Sc_3N@C_{78}$[29] is denoted by an asterisk.

$Sc_3N@C_{80}$ (II)[22] and $Sc_3N@C_{78}$.[29] The infrared selection rules for the C_{78} and C_{80} IPR isomers are given in Table 2. Almost identical vibrational structures of $Sc_3N@C_{80}$ (I) and $Tm_3N@C_{80}$ (I), and of $Sc_3N@C_{80}$ (II) and $Tm_3N@C_{80}$ (II), respectively, are evident from Figure 6. The detailed analysis leads to five groups of tangential cage modes for both C_{80} (I) isomers, labelled as B, C, D, F and H according to references [15,22] and one strong radial cage mode around

Table 2. Infrared selection rules for the five IPR isomers of C_{78} and the seven IPR isomers of C_{80} fullerene. For C_{2v} isomers the axes were defined that more atoms are located in the (yz) mirror plane than in the (xz) plane.

Cage isomer[30]	Symmetry group	IR active vibrations
C_{78}:1	D_3	37 A_2 + 76 E
C_{78}:2	C_{2v}	59 A_1 + 56 B_1 + 57 B_2
C_{78}:3	C_{2v}	60 A_1 + 56 B_1 + 57 B_2
C_{78}:4	D_{3h}	20 A_2'' + 38 E′
C_{78}:5	D_{3h}	19 A_2'' + 37 E_1'
C_{80}:1	D_{5d}	12 A_{2u} + 23 E_{1u}
C_{80}:2	D_2	58 B_1 + 58 B_2 + 58 B_3
C_{80}:3	C_{2v}	62 A_1 + 57 B_1 + 59 B_2
C_{80}:4	D_3	38 A_2 + 78 E
C_{80}:5	C_{2v}	61 A_1 + 57 B_1 + 59 B_2
C_{80}:6	D_{5h}	13 A_2'' + 23 E_1'
C_{80}:7	I_h	6 F_{1u}

500 cm^{-1}. The number of lines within these groups is slightly larger for $Tm_3N@C_{80}$ (I) than for $Sc_3N@C_{80}$ (I), most notably in the tangential mode groups C and F, and for the strong radial cage mode. Some weak lines in the Sc_3N spectrum have medium intense counterparts in the $Tm_3N@C_{80}$ (I) spectrum. This is particularly apparent in the tangential mode group D. The FTIR spectra of the C_{80} (II) isomers have signatures similar to the C_{80} (I) isomers, and their most intense line groups are closely related to those of the C_{80} (I) isomers. The tangential mode groups A and I of $Tm_3N@C_{80}$ (II) and $Sc_3N@C_{80}$ (II) are not present in the spectra of the first isomers, and the line groups F have significantly lower intensities in the C_{80} (II) than in both C_{80} (I) isomer spectra. Similar to the tendency seen for the C_{80} (I) isomers, the line group splitting is stronger for $Tm_3N@C_{80}$ (II) than for $Sc_3N@C_{80}$ (II), and some weak $Sc_3N@C_{80}$ (II) lines correspond to medium intense lines in the $Tm_3N@C_{80}$ (II) spectrum. The total numbers of infrared active lines, including all lines with relative intensities from 100% down to 2%, are 39 and 46 cage modes for $Tm_3N@C_{80}$ (I) and $Tm_3N@C_{80}$ (II), respectively. These numbers are higher than those found in $Sc_3N@C_{80}$ (I) and $Sc_3N@C_{80}$ (II) by approximately 10.[22] According to the selection rules (Table 2), only the highest symmetric C_{80} cage isomers C_{80}:1, C_{80}:6, and C_{80}:7 can account for the small number of infrared active lines. The final isomer assignment is based on the close spectral resemblance with their $Sc_3N@C_{80}$ counterparts: $Tm_3N@C_{80}$ (I) is assigned to the C_{80} isomer C_{80}:7 with I_h symmetry, and $Tm_3N@C_{80}$ (II) is assigned to C_{80}:6 (D_{5h}). Schematic structure models of both $Tm_3N@C_{80}$ isomers are shown in Figure 7.

There is one major difference between the $Tm_3N@C_{80}$ and the $Sc_3N@C_{80}$ infrared spectra. The strongest low-energy infrared line of $Tm_3N@C_{80}$ (I and II) was found at approximately 710 cm^{-1}, that is, at ~110 cm^{-1} higher than for $Sc_3N@C_{80}$ (I and II). For the $Sc_3N@C_{80}$ clusterfullerenes, this line was assigned to the antisymmetric ScN stretching vibration of the Sc_3N cluster.[15,22] Due to their comparably high intensities and their strong metal dependences, the $Tm_3N@C_{80}$ lines around 710 cm^{-1} are assigned to the antisymmetric thulium–nitrogen stretching mode, ν_{as}(TmN). The detailed analysis of ν_{as}(TmN) and its implications for the geometric and electronic structure of the Tm_3N cluster is subject of further investigations.

In contrast to the FTIR spectra of $Tm_3N@C_{80}$ and $Sc_3N@C_{80}$ (I, II), those of $Tm_3N@C_{78}$ and $Sc_3N@C_{78}$ show significant differences from each other (Figure 6). Both spectra exhibit several prominent lines, indicated by dotted arrows, that are completely absent in the other spectrum. Therefore, identical C_{78} cage isomers can be excluded. By using a line fit model, 60 infrared active lines were found for $Tm_3N@C_{78}$ within a range of relative intensities from 2 to 100%. This is very close to the number of infrared active modes of the two highest symmetric C_{78} cages C_{78}:4 (D_{3h}) and C_{78}:5 (D_{3h}) (see Table 2). On the other hand this number is larger than the number of $Sc_3N@C_{78}$ infrared lines. As 173 and 174 modes are infrared allowed for the C_{2v} isomers C_{78}:2 and C_{78}:3, both cages are excluded as possible structures of

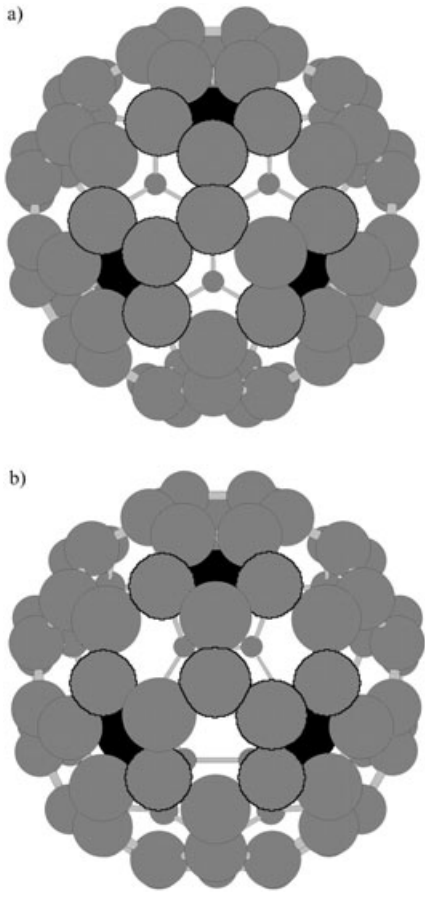

Figure 7. Schematic structure models of a) $Tm_3N@C_{80}$ (I; I_h) and b) $Tm_3N@C_{80}$ (II; D_{5h}); the thulium atoms are drawn in black, the carbon atoms are in grey and the nitrogen atoms are hidden by the central carbon atoms; trigonal planar geometry and orientation of the Tm_3N cluster are still to be confirmed.

$Tm_3N@C_{78}$. The cage C_{78}:5 (D_{3h}), previously found for $Sc_3N@C_{78}$, can also be excluded due to the significant differences in the FTIR spectra of $Tm_3N@C_{78}$ and $Sc_3N@C_{78}$. Hence the cage isomers C_{78}:1 (D_3) or C_{78}:4 (D_{3h}) are the two possible carbon cages of $Tm_3N@C_{78}$. Their ellipsoidal shape could account for the significant larger HPLC retention time compared to $Sc_3N@C_{78}$. The conclusion is also consistent with the visible-NIR analysis. The final isomer assignment is a matter of forthcoming spectroscopic and theoretical investigations.

Conclusion

A new family of trimetal nitride clusterfullerenes, the $Tm_3N@C_{2n}$ ($39 \leq n \leq 43$) family, has been explored. It is the largest clusterfullerene family characterised so far. As in the Sc_3N family, the C_{80}-based $Tm_3N@C_{80}$ isomers (I: I_h and II: D_{5h}) were formed in the greatest abundance. Trimetal nitride clusterfullerenes with cages greater than C_{80} were isolated for the first time. All isolated Tm_3N structures were classified as large energy-gap fullerenes. The observed

energy-gap ordering could partly account for the ordering of the observed abundances. The idea of a general coexistence of two C_{80} cage isomers of I_h and D_{5h} symmetry in trimetal nitride clusterfullerene samples was supported by this study. For $Tm_3N@C_{78}$ clusterfullerene a carbon cage structure different from that of $Sc_3N@C_{78}$ was established. The analysis pointed to an elliptical carbon cage, with C_{78}:1 (D_3) or C_{78}:4 (D_{3h}) being the probable structures.

Experimental Section

The fullerene soot was prepared by a modified Krätschmer–Huffman arc burning method. Mixtures of thulium metal or oxide and graphite powder were pressed into the holes of graphite rod electrodes in a molar ratio of 1:12.5. As source of nitrogen 20 mbar NH_3 were added to the reactor atmosphere of 200 mbar He.[12–14] Non-fullerene hydrocarbon by-products were extracted from the soot with acetone. The as purified soot was soxhlet extracted by CS_2 for 20 h. On average 500 μg fullerenes were obtained per burning. In this process approximately 3 g of carbon rods were consumed. Fullerene separation was done by multistage high performance liquid chromatography (HPLC) with pure toluene as the eluent. In the first stage, the soot extract was separated into three fractions by using a linear combination of two analytical 4.6×250 mm BuckyPrep columns (Nacalai Tesque). $Tm_3N@C_{80}$ (I) and $Tm_3N@C_{80}$ (II) were isolated in 1 to 2 runs from the first fraction using a flow rate of 1.6 mL min^{-1} and an injection volume of 250 μL. $Tm_3N@C_{78}$ and $Tm_3N@C_{82}$ were isolated from fraction 2 by two stages on a semi-preparative 10×250 mm Buckyclutcher column applying a flow rate of 1 mL min^{-1}, and an injection volume of 100 μL. $Tm_3N@C_{84}$ and $Tm_3N@C_{86}$ were isolated from the third fraction by one additional step on the BuckyPrep columns and another on the BuckyClutcher column. A UV detector set to 320 nm was used for fullerene detection. The purities of the isolated samples were checked by HPLC runs and laser desorption time-of-flight (LD-TOF) mass spectrometry analysing both, negative and positive ions. The following clusterfullerene amounts were isolated in our study by processing a 10 mg fullerene extract: 2 mg $Tm_3N@C_{80}$ (I), 400 μg $Tm_3N@C_{80}$ (II), 150 μg $Tm_3N@C_{78}$, 200 μg $Tm_3N@C_{84}$, 50 μg $Tm_3N@C_{82}$, and 100 μg $Tm_3N@C_{86}$. Visible-NIR spectra of clusterfullerene solutions in toluene were recorded on a UV-visible-NIR 3101-PC spectrometer (Shimadzu, Japan) by using quartz cells of 1 mm layer thickness. For FTIR measurements $Tm_3N@C_{80}$ (I and II; 200 μg) and $Tm_3N@C_{78}$ (150 μg) dissolved in toluene (1 mL) were used to drop-coat KBr single-crystal disks. Residual solvent was removed by heating the polycrystalline films in a vacuum of 2×10^{-6} mbar at 235 °C for 3 h. The FTIR spectra were recorded at room temperature on an IFS 66v spectrometer (Bruker, Germany). These three Tm_3N clusterfullerenes were isolated in sufficiently high yields and were stable in the solid state. $Tm_3N@C_{84}$ proved to be less stable in solid form, and the isolated amounts of $Tm_3N@C_{82}$ and $Tm_3N@C_{86}$ were too small for a reliable FTIR analysis.

Acknowledgement

The authors cordially thank H. Zöller, S. Döcke and K. Kojucharow for technical assistance in the fullerene production, HPLC separation and spectroscopic measurements. J.W. would like to thank the IAESTE student exchange program for supporting her work at the IFW Dresden.

[1] H. Shinohara, *Rep. Prog. Phys.* **2000**, *63*, 843–892.
[2] *Endofullerenes: A New Family of Carbon Clusters* (Eds.: T. Akasaka, S. Nagase), Kluwer Academic, Dordrecht, Boston, London, **2002**.
[3] P. Kuran, M. Krause, A. Bartl, L. Dunsch, *Chem. Phys. Lett.* **1998**, *292*, 580–586.
[4] C. R. Wang, T. Kai, T. Tomiyama, T. Yoshida, Y. Kobayashi, E. Nishibori, M. Takata, M. Sakata, H. Shinohara, *Nature* **2000**, *408*, 426–427.
[5] U. Kirbach, L. Dunsch, *Angew. Chem.* **1996**, *108*, 2518–2521; *Angew. Chem. Int. Ed. Engl.* **1996**, *35*, 2380–2383.
[6] T. Pichler, M. S. Golden, M. Knupfer, J. Fink, U. Kirbach, P. Kuran, L. Dunsch, *Phys. Rev. Lett.* **1997**, *79*, 3026–3029.
[7] T. Almeida-Murphy, T. Pawlik, A. Weidinger, M. Höhne, R. Alcala, J.-M. Spaeth, *Phys. Rev. Lett.* **1996**, *77*, 1075–1078.
[8] P. Jakes, K. P. Dinse, C. Meyer, W. Harneit, A. Weidinger, *Phys. Chem. Chem. Phys.* **2003**, *5*, 4080–4083; M. Kanai, K. Porfyrakis, A. D. Briggs, T. J. S. Dennis, *Chem. Commun.* **2004**, 210–211.
[9] H. Shinohara, M. Inakuma, N. Hayashi, H. Sato, Y. Saito, T. Kato, S. Bandow, *J. Phys. Chem.* **1994**, *98*, 8597–8599.
[10] A. Bartl, L. Dunsch, *Synth. Met.* **2001**, *121*, 1147–1148.
[11] S. Stevenson, G. Rice, T. Glass, K. Harich, F. Cromer, M. R. Jordan, J. Craft, E. Hajdu, R. Bible, M. M. Olmstead, K. Maitra, A. J. Fisher, A. L. Balch, H. C. Dorn, *Nature* **1999**, *401*, 55–57.
[12] L. Dunsch, P. Georgi, F. Ziegs, H. Zöller, German patent DE 10301722 A1.
[13] L. Dunsch, P. Georgi, M. Krause, C. R. Wang, *Synth. Met.* **2003**, *135/136*, 761–762.
[14] L. Dunsch, M. Krause, J. Noack, P. Georgi, *J. Phys. Chem. Solids* **2004**, *65*, 309–315.
[15] M. Krause, H. Kuzmany, P. Georgi, L. Dunsch, K. Vietze, G. Seifert, *J. Chem. Phys.* **2001**, *115*, 6596–6605.
[16] M. M. Olmstead, A. de Bettencourt-Dias, J. C. Duchamp, S. Stevenson, D. Marciu, H. C. Dorn, A. L. Balch, *Angew. Chem.* **2001**, *113*, 1263–1265; *Angew. Chem. Int. Ed.* **2001**, *40*, 1223–1225.
[17] S. Stevenson, P. W. Fowler, T. Heine, J. C. Duchamp, G. Rice, T. Glass, K. Harich, E. Hajdu, R. Bible, H. C. Dorn, *Nature* **2000**, *408*, 427–428.
[18] L. Feng, J. X. Xu, Z. J. Shi, X. R. He, Z. N. Gu, *Chem. J. Chin. Univ.* **2002**, *23*, 996–998.
[19] E. B. Iezzi, J. C. Duchamp, K. R. Fletcher, T. E. Glass, H. C. Dorn, *Nano Lett.* **2002**, *2*, 1187–1190; S. Stevenson, H. M. Lee, M. M. Olmstead, C. Kozikowski, P. Stevenson, A. L. Balch, *Chem. Eur. J.* **2002**, *8*, 4528–4535.
[20] M. M. Olmstead, A. de Bettencourt-Dias, J. C. Duchamp, S. Stevenson, H. C. Dorn, A. L. Balch, *J. Am. Chem. Soc.* **2000**, *122*, 12220–12226.
[21] J. C. Duchamp, A. Demortier, K. R. Fletcher, D. Dorn, E. B. Iezzi, T. Glass, H. C. Dorn, *Chem. Phys. Lett.* **2003**, *375*, 655–659.
[22] M. Krause, L. Dunsch, *ChemPhysChem* **2004**, *5*, 1445–1449.
[23] D. Fuchs, H. Rietschel, R. H. Michel, A. Fischer, P. Weis, M. M. Kappes, *J. Phys. Chem.* **1996**, *100*, 725–729.
[24] K. Kikuchi, K. Akiyama, K. Sakaguchi, T. Kodama, H. Nishakawa, I. Ikemoto, T. Ishigaki, Y. Achiba, K. Sueki, H. Nakahara, *Chem. Phys. Lett.* **2000**, *319*, 472–476.
[25] M. Inakuma, E. Yamamoto, T. Kai, Ch. R. Wang, T. Tomiyama, H. Shinohara, T. J. S. Dennis, M. Hulman, M. Krause, H. Kuzmany, *J. Phys. Chem. B* **2000**, *104*, 5072–5077.
[26] N. Tagmatarchis, H. Shinohara, *Chem. Mater.* **2000**, *12*, 3222–3226.
[27] Ch.-R. Wang, M. Inakuma, H. Shinohara, *Chem. Phys. Lett.* **1999**, *300*, 379–384.
[28] N. Tagmatarchis, E. Aslanis, K. Prassides, H. Shinohara, *Chem. Mater.* **2001**, *13*, 2374–2379.
[29] P. Georgi, Ph.D. thesis, Dresden, **2004**.
[30] P. W. Fowler, D. E. Manolopoulos, *An Atlas of Fullerenes*, Clarendon, Oxford, **1995**.

Received: July 2, 2004
Published online: December 3, 2004

